


Direct observation of the fracture behavior of the polyether ketone ketone (PEKK) spherulites

Vanessa Marinosci^{1,2} | Kuan Chen³ | Nick G. J. Helthuis¹ |
 Wouter J. B. Grouve¹ | Erik G. de Vries¹ | Ningzhong Bao³ |
 Remko Akkerman^{1,2} | Matthijn B. de Rooij¹ | Liangyong Chu^{1,3} 

¹Department of Mechanics of Solids, Surfaces and Systems, Faculty of Engineering Technology, University of Twente, Enschede, The Netherlands

²ThermoPlastic composites Research Center (TPRC), Enschede, The Netherlands

³State Key Laboratory of Materials-Oriented Chemical Engineering, College of Chemical Engineering, Nanjing Tech University, Nanjing, China

Correspondence

Liangyong Chu, Department of Mechanics of Solids, Surfaces and Systems, Faculty of Engineering Technology, University of Twente, 7500 AE Enschede, The Netherlands.

Email: l.chu@njtech.edu.cn

Funding information

HTSM2017, Grant/Award Number: 16213; National Key Research and Development Program of China, Grant/Award Number: 2020YFE0100100

Abstract

This article reports the direct observation of the fracture of individual poly-ether-ketone-ketone (PEKK) spherulites. A single layer of PEKK spherulites was obtained by bonding a PEKK film in-between two sandblasted Ti alloy plates using an autoclave. The crack of an individual PEKK spherulite was achieved by opening the Ti/PEKK/Ti sandwich using a double cantilever beam test. The fracture morphology of the PEKK spherulite was characterized using scanning electron microscopy and atomic force microscopy. It was found that under tensile stress the crack of the individual spherulite propagates along the middle plane and crosses the nucleation core. This is due to the symmetric radial structure of the spherulite. Moreover, it was found that the fracture surface morphology at the core of the spherulite is strongly influenced by the local crystalline structure, which is anisotropic and determined by the initial nucleation growth direction. As a result, the area fraction experiencing plastic deformation during the fracture of PEKK spherulites at different orientations may vary by an order of 10. Our results show the important role of the initial nucleation growth direction on the mechanical properties of the polymer crystals and may provide a new approach to the design of high-performance polymer materials with tailored crystalline structures.

KEYWORDS

AFM, anisotropic, fracture, individual spherulite, lamella packing, nucleation structure

1 | INTRODUCTION

The poly-aryl-ether-ketone (PAEK) polymers and their composites have drawn increasing attention in various fields, such as biomedical devices, implants, electronic packages, and fiber-reinforced composites, due to the high mechanical strength and modulus, good chemical stability,

and high thermal resistance.^{1–4} The PAEK polymers such as polyether ether ketone (PEEK) and polyether ketone ketone (PEKK) are semi-crystalline polymers. In the past decades, the crystallization kinetics of PAEK polymers and the structure–performance relationships have been extensively studied and it has been demonstrated that the crystalline structures play an important role in the performance of PAEK polymers and their composites.^{5–9}

Studies about the relationships between crystalline structure and the mechanical performance of PAEK

Vanessa Marinosci and Kuan Chen contributed equally to this paper and should be considered the co-first authors.

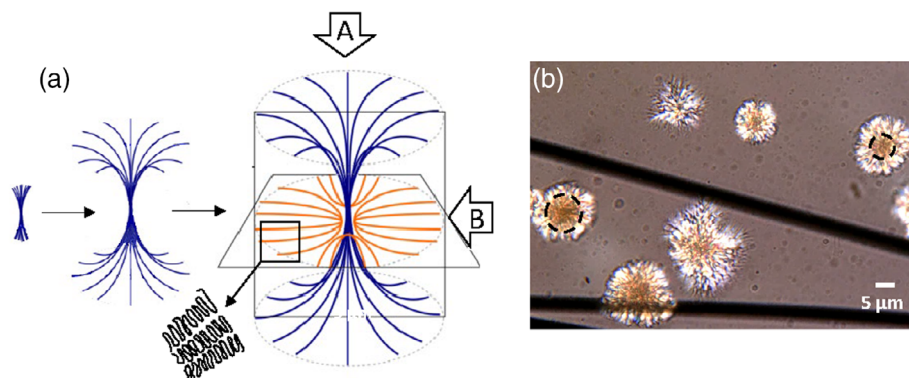


FIGURE 1 (a) Schematic drawing of the formation of a polymer spherulite. The microstructures at the core of the spherulite in different planes marked as A and B are different. (b) Hot stage polarized light optical image of polyether ketone spherulites. The structure at the core of the different spherulites varies due to the different directions of the nucleation site of the spherulite core. [Color figure can be viewed at [wileyonlinelibrary.com](https://onlinelibrary.wiley.com/doi/10.1002/app.54764)]

polymers had been mainly focused on multiple spherulites.¹⁰ Spherulites, composed of radially directed crystal fibrils, are the basic building blocks for a wide range of material systems such as semi-crystalline polymers, synthetic ceramics, minerals, and ice.^{11,12} The structure of the polymer spherulites has been well described as dense, spherical crystal gatherings. To develop such a structure, a single nucleation site in the form of a single lamella first grows to a hedrite, then a sheaf, and finally a spherulite as shown in Figure 1a.¹³ At the macroscale level, polymer spherulites are considered as dense and isotropic building blocks and play an important role in the mechanical properties of polymers such as yield strength and fatigue behavior and inter-spherulite fracture behavior dominates the failure of these materials.^{14–18} At the microscale, the local structure of the spherulite needs to be considered, i.e. the inner nucleation site is anisotropic while the outer ring part is isotropic.^{6,19–21} As shown in Figure 1, the structure of a spherulite in different planes (or view from different directions) is different. Thus, the crack behavior is strongly influenced by the planes that the crack is located in. Various researchers have demonstrated that the anisotropic structure of the polymer spherulite at the microscale plays an important role in the thermal, electrical, and gas permeability properties of the semi-crystalline polymers, which is crucial for their applications in composites, semiconductors, nano-devices, membranes, and coatings.^{22–29} Until now, studies on the spherulite structure–performance relationships of semi-crystalline PAEK polymers on the microscale, mainly consider multiple spherulites. For example, Bretz studied the influence of local morphology of spherulites on the crack propagation of polycaprolactone, poly(1-butene) and polyamide 6 by stretching of the polymer film specimen. It was reported that the crack started at the core region of the spherulites and extended towards the periphery.³⁰ Thomas et al found that the size of the spherulites had an influence on the crack behavior of semi-crystalline polymers by fracture of a polymer film.³¹ The spherulites with a larger size showed more

plastic deformation during a crack while the smaller spherulites were more brittle. Chu et al reported the study on the failure behavior of PEEK samples using a compact tension test and found that spherulite size had a profound influence on the fracture mechanism.¹⁰ Until now, research on individual spherulites is limited.³² One of the challenges is the lack of experimental methodologies to directly observe the crack behavior at individual spherulite scales.

In our previous work, the fracture behavior of a titanium and PEKK interface has been studied.²¹ It showed that the local structure of the PEKK spherulite formed at the contact with the titanium (Ti) surface dominates the fracture behavior of the interface. When cohesive failure occurs, the opening of a single PEKK spherulite was realized, and a brittle failure at the spherulite core and a ductile failure at the spherulite edge was recognized.²¹ Inspired by these results, in this article, direct observation of the fracture behavior of spherulitic structures on the individual spherulite level is reported. To study the crack behavior of an individual PEKK spherulite, it is needed to (i) prepare PEKK material with a monolayer of spherulites and (ii) hold the individual spherulite and apply a pulling force to open it. Herein, the sample to enable the crack at an individual spherulite level was designed. By applying a pulling force on a thin PEKK film composed of a single layer of PEKK spherulites, the crack occurs at the core and opens the spherulites, which enables the direct observation of the fracture of crystalline structures at an individual spherulite level. It has been demonstrated that the fracture surfaces show an anisotropic fracture behavior, the plastic deformation region of an individual spherulite with respect to the intra-lamella failure, may vary by a factor of 10 and is determined by the direction of the nucleation site with respect to the applied force. Our results provide a deeper understanding of the fracture behavior of a spherulite and may yield a new approach to preparing high-performance crystalline structures by tailoring the nucleation site direction, e.g. using 2D nucleation agents.

2 | EXPERIMENTAL SECTION

2.1 | Preparation of the sandblasted Ti alloy plates

In this study, two sandblasted Ti alloy plates were used as the gripper to fix and open the spherulites. Grade 5 titanium (Ti6Al4V) plates with a thickness of 3 mm, provided by Singeling B.V., were used. The surface morphology of the titanium strips was modified via sand-blasting treatment before sample manufacturing. The detailed settings of the grit-blasting treatment can be found in our previous article.^{21,33}

2.2 | Sample preparation of the Ti/PEKK/Ti sandwich for the double cantilever beam (DCB) test

To fix and open the spherulites, the Ti/PEKK/Ti sandwich was prepared. This Ti/PEKK/Ti sandwich was prepared by bonding a layer of PEKK between two Ti strips, whose dimensions were $190 \times 20 \times 3 \text{ mm}^3$. The stack was placed in a steel frame, the steel frame ensured a good alignment of the two titanium strips during the co-consolidation process and reduced the polymer flow. To open the sandwich using the DCB test, an initial pre-crack at one of the two titanium/PEKK interfaces is required, which was introduced by applying a mold release agent (Marbocote 227-CEE) on the first 60 mm of the titanium surface prior to the consolidation. The same release agent was also applied to the steel frame to avoid bonding to the polymer. The sample was consolidated using a slow process, carried out in an autoclave. The thermal cycle used was comparable to the cycle adopted to consolidate TPCs laminates based on PEKK polymer. First, the sample was heated up to a temperature of 375°C and then a dwell time of 30 min and 6 bar pressure were applied. Afterward, the system was cooled down at a constant rate of $4^\circ\text{C}/\text{min}$.

The DCB test was conducted using a Zwick universal testing machine. The tensile load was applied by bonding two loading blocks at the end of the titanium/PEKK/titanium sample, in correspondence to the pre-crack region. The force was measured using a 2.5 kN load cell, while the displacement was evaluated via a 150 mm linear variable displacement transducer (LVDT). The test was performed at a constant displacement rate of 3 mm/min.

2.3 | Preparation of the crystallized PEKK film sample

To prepare crystallized PEKK film sample with nucleation site initiating on the surface of the polymer melts and

further growing to a spherulite, a THMS600 hot stage purchased from Linkam Scientific Instruments has been used to prepare the sample. A $5 \times 5 \text{ mm}$ PEKK film was placed on a glass plate, after being heated up to 375°C and a dwelling time of 10 minutes, the heater is turned off and the PEKK melt is cooled down to room temperature using the compressed air. During the cooling, the temperature on the polymer surface is lower than the bulk, thus, the nucleation site first occurs on the PEKK surface.

2.4 | Characterization methods

The atomic force microscopy (AFM) morphology characterization is performed using a Park XE-100 AFM from Park Systems using an ACTA AFM probe purchased from AppNano. The spring constant of the probe is 26 N m^{-1} determined using the thermal noise method.^{34–36} A Sensofar S Neox confocal microscopy is used for all the optical microscopy characterizations.

The scanning electron microscope (SEM) (Jeol JSM-7200f) has been used to investigate the polymer microstructure at the crack surface. A gold layer of a few nanometers has been applied before conducting the SEM characterizations. The high-resolution SEM image was taken using a ZEISS MERLINSEM in MESA+ at the University of Twente. No conductive coating has been applied before the characterizations.

3 | RESULTS AND DISCUSSIONS

3.1 | Morphology characterization of the fracture surface

Figure 2a shows the schematic drawing of the setup designed to study the crack behavior of an individual PEKK spherulite. To obtain the monolayer PEKK spherulites, a PEKK film with a thickness of $40 \mu\text{m}$ was prepared by placing the Kepstan[®] $50 \mu\text{m}$ 7002 PEKK film, produced by Arkema, in between two Ti plates. Limited squeeze flow during processing in the autoclave led to a final PEKK film thickness of $40 \mu\text{m}$. Our previous studies on the crystallization of PEKK 7002 materials showed that the average diameter of the PEKK spherulites, and thus the average distance between two nuclei, is about $42 \mu\text{m}$ when PEKK 7002 cools down from 385°C at a cooling rate of $4^\circ\text{C}/\text{min}$.^{37,38} Therefore, as shown in Figure 2b, a film thickness of $40 \mu\text{m}$ allows only one nucleation site in the thickness direction, thereby obtaining a monolayer of PEKK spherulites between the two Ti plates.

Sandblasted Ti grade 5 alloy plates were used to hold the individual spherulite and to apply a pulling force to

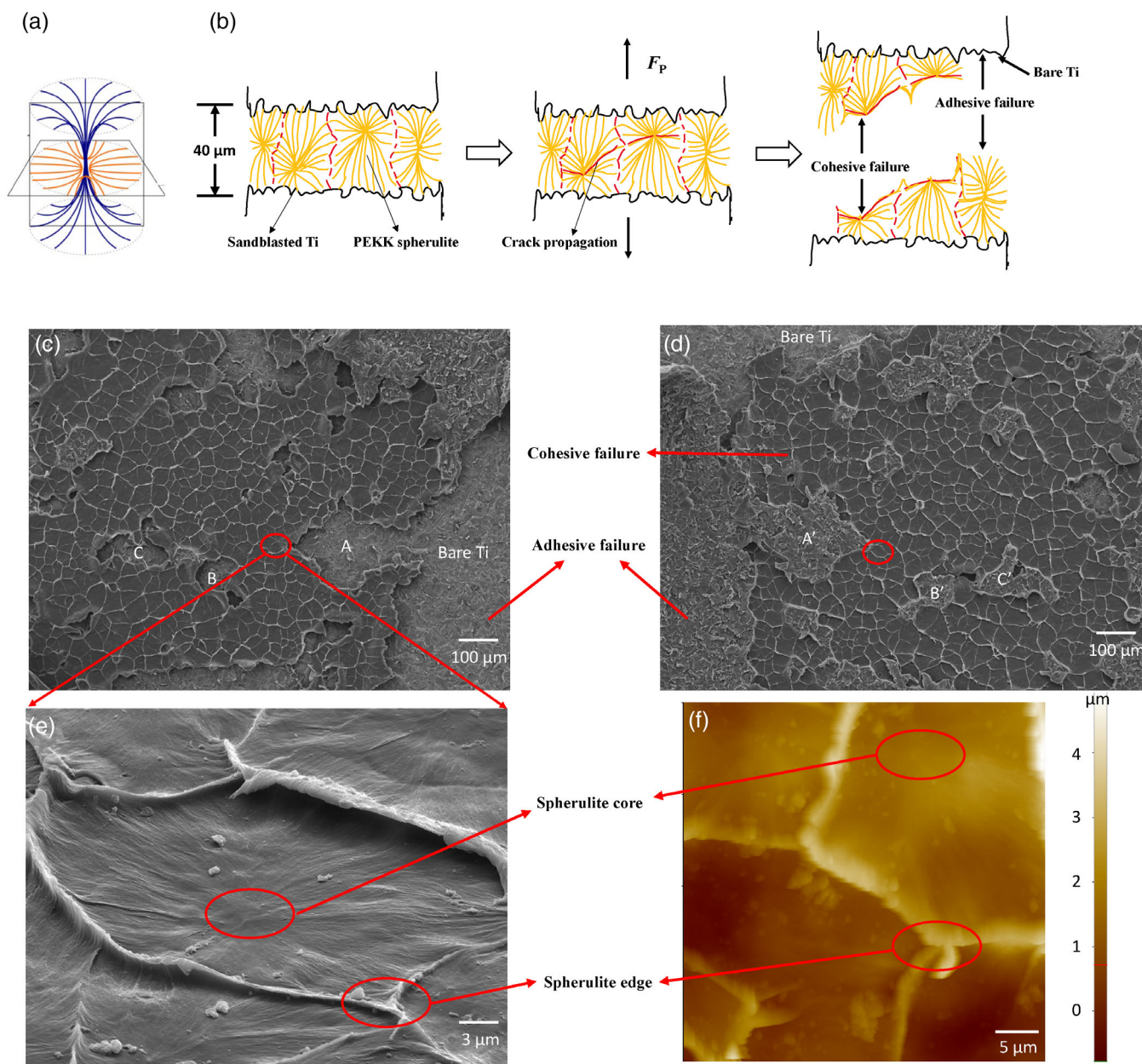


FIGURE 2 (a) Schematic drawing of the 3D structure of a spherulite. (b) Schematic drawing of the opening of monolayer polyether ketone (PEKK) spherulites using the sandblasted Ti plates as the gripper. (c) Scanning electron microscopy (SEM) image of the fracture surface after the opening of the PEKK spherulites. The mirror side of the surface in (c) is shown in (d). (e) The higher magnification SEM image of the region marked as a red circle in (c). (f) Atomic force microscopy height morphology of the PEKK spherulite fracture surface. [Color figure can be viewed at wileyonlinelibrary.com]

open it, as is shown in Figure 2b. In our previous article, we reported that after roughening the titanium surface via sandblasting, the interfacial bonding between Ti and PEKK is larger than the strength of PEKK, which means a crack occurs in the polymer region when opening the Ti/PEKK joint. Therefore, in this work, the two Ti plates were sandblasted to ensure cohesive failure, and hence, failure within the spherulite layer of the Ti/PEKK/Ti sandwich, as schematically shown in Figure 2b. This type of

sample was prepared using an autoclave and opened using the DCB method. Figure 2c shows the SEM image of the fracture surface of the Ti/PEKK/Ti sandwich after the DCB test. The black regions with irregular shapes are the spherulites after a fracture. The whiter regions are the bare Ti plates region after an adhesive failure. Figure 2c is the counterpart of Figure 2d after the opening of the sandwich. The shape of the regions marked as A, B, and C is the same as the shape of the regions A', B', and C'. Therefore,

Figure 2c,d are the mirror images of each other, which indicates that the single-layer PEKK spherulites have been opened from the middle using the designed method. Figure 2e shows the high-resolution SEM image of a spherulite after a fracture. The spherulite with a radial structure was recognized. The spherulite will most likely crack in its midplane normal to the applied stress. This is because here the lamellar crystals grow parallel to the plane, thereby inducing weak points as the inter-lamella strength is lower than the intra-lamella strength.^{11,38,39} Regions with more deformations are found at the edge of the spherulite probably due to its more amorphous nature, as shown in Figure 2e,f. These results show that the fracture of a PEKK spherulite includes multiple mechanisms. As shown below, more characterizations were performed to further describe the fracture behavior of a PEKK spherulite.

3.2 | Determination of the microstructure of the fracture surface

To determine the local structure at the core and edge regions of the fracture surface as shown in Figure 2e,f, the microstructure of these regions was characterized using tapping mode AFM. In tapping mode AFM, the phase shift of the oscillating cantilever is sensitive to the material properties such as hardness and modulus.^{40,41} For semi-crystalline polymers, the crystalline region is harder than the amorphous region, thus, phase mode AFM has been used as a tool to characterize the local crystalline structures.^{38,42} Figure 3a shows the AFM height morphology of the core region of the spherulite after a fracture. Figure 3b shows the AFM phase image corresponding to Figure 3a. The higher magnification AFM height and phase images of both the core region and radial structure region, as marked in the white square in Figure 3a,b, were shown in Figure 3a1,b1,a2,b2, respectively.

As shown in Figure 3b, the core region surrounded by radial structures was recognized. Considering the mirror structure as shown in Figure 2c,d, the polymer morphology identified in Figure 3a corresponds to opening of a spherulite from its middle plane. As shown in Figure 3b1,b2, PEKK crystalline structure with a width of about 20 nm was recognized. This is of the same size as the PEKK lamellar crystals we reported before.³⁷ Herein, it is concluded that when individual PEKK spherulite is opened by a pulling force, fracture tends to initiate at the middle plane and the fracture behavior at the crystalline core is different from the surrounding regions with radial crystalline structure.

To further describe the fracture behavior of an PEKK spherulite, the fracture morphology at the edge region of the spherulite was characterized using tapping mode AFM as shown in Figure 4. Figure 4b shows the AFM

height morphology of the edge region of the spherulite after a fracture. More plastic deformation was recognized in this region. From the corresponding phase image as shown in Figure 4c, it is found that the directions of the PEKK crystals are different, which indicates a different crystalline structure in this region.

To further understand the higher plastic deformation at the joining part of two spherulites, the crystalline structure of this part was characterized. Two Spherulites crystallized from the surface was used to simulate the contact of two spherulites in the bulk as shown in Figure 5a (the preparation of the samples can be found in Section 2.3). As shown in the higher resolution image in Figure 5b, the interlocking of lamellar crystals from two adjacent spherulites was recognized. This may lead to a lower density of crystallinity and higher intermolecular forces between lamellar crystals, as a result, higher plastic deformation occurs after opening of the spherulite.

In Figure 2c,d, adhesive failure between Ti plate and PEKK was also recognized. The PEKK surface in this region was characterized using tapping mode AFM as shown in Figure 6b,c. Lamellar crystalline structure with a width of about 20 nm was also recognized. The fracture behavior was different from the cohesive failure region, this indicates the successful opening of the PEKK spherulites from the middle.

3.3 | Anisotropic fracture behavior of the PEKK spherulites

As shown in Figure 1 and mentioned above, the microstructure of a PEKK spherulite is anisotropic. This is the result of the random direction of the nucleation site and the growth nature of an spherulite. Herein, the anisotropic structure of a PEKK spherulite was confirmed by characterizing the crystalline structure of the surface crystallized PEKK spherulite by using SEM, AFM, and optical microscopy, as shown in Figure 7a–c, respectively. For a PEKK thin film formed by multiple PEKK spherulites, the initial PEKK nucleation directions are randomly distributed.

Figure 7b shows the AFM height morphology of the PEKK crystallized on a thin glass plate. The radial structure of a PEKK spherulite can be recognized. The PEKK spherulite has an anisotropic structure, which is further confirmed by the high-resolution SEM image shown in Figure 7a. For instance, the crystalline packing structure along the two directions marked as directions 1 and 2 are different. Thus, when applying pulling force and opening the spherulite, the direction of crack propagation may vary depending on the direction of the external pulling force with respect to the internal spherulite structures.

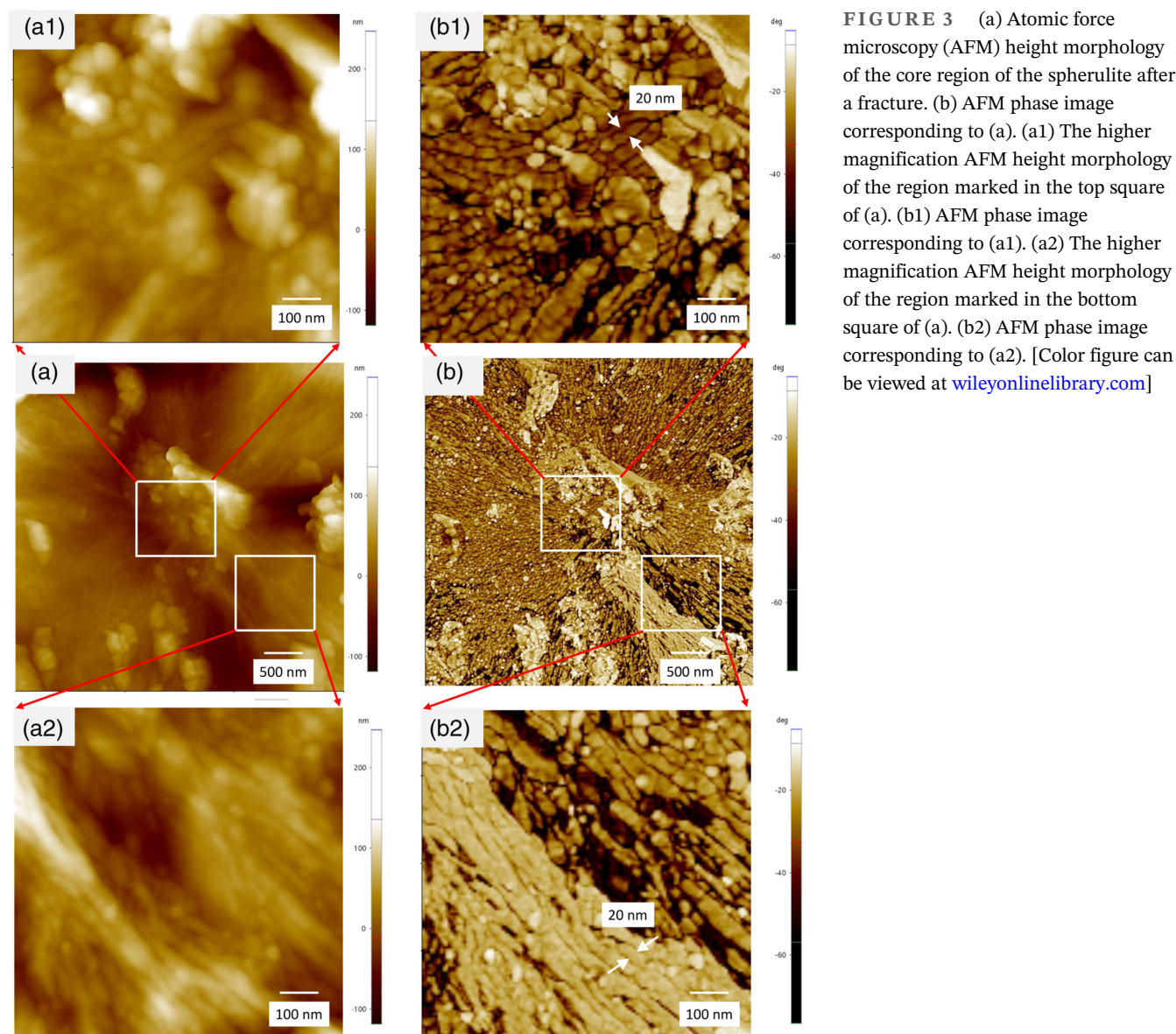


FIGURE 3 (a) Atomic force microscopy (AFM) height morphology of the core region of the spherulite after a fracture. (b) AFM phase image corresponding to (a). (a1) The higher magnification AFM height morphology of the region marked in the top square of (a). (b1) AFM phase image corresponding to (a1). (a2) The higher magnification AFM height morphology of the region marked in the bottom square of (a). (b2) AFM phase image corresponding to (a2). [Color figure can be viewed at wileyonlinelibrary.com]

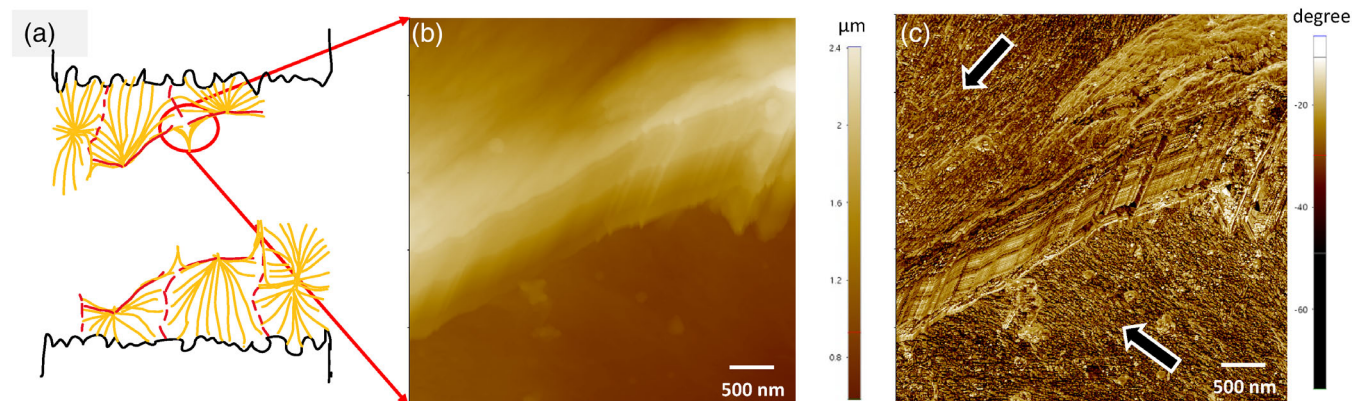


FIGURE 4 (a) Schematic drawing of the fracture of single layer polyether ketone spherulites. (b) Atomic force microscopy (AFM) height morphology of the edge region of the spherulite after a fracture. (c) AFM phase image corresponding to (b). [Color figure can be viewed at wileyonlinelibrary.com]

FIGURE 5 (a) Atomic force microscopy (AFM) height morphology of the crystallized polyether ketone ketone (PEKK) film surface. (b) High resolution AFM height morphology of the joining region between two PEKK spherulites. [Color figure can be viewed at wileyonlinelibrary.com]

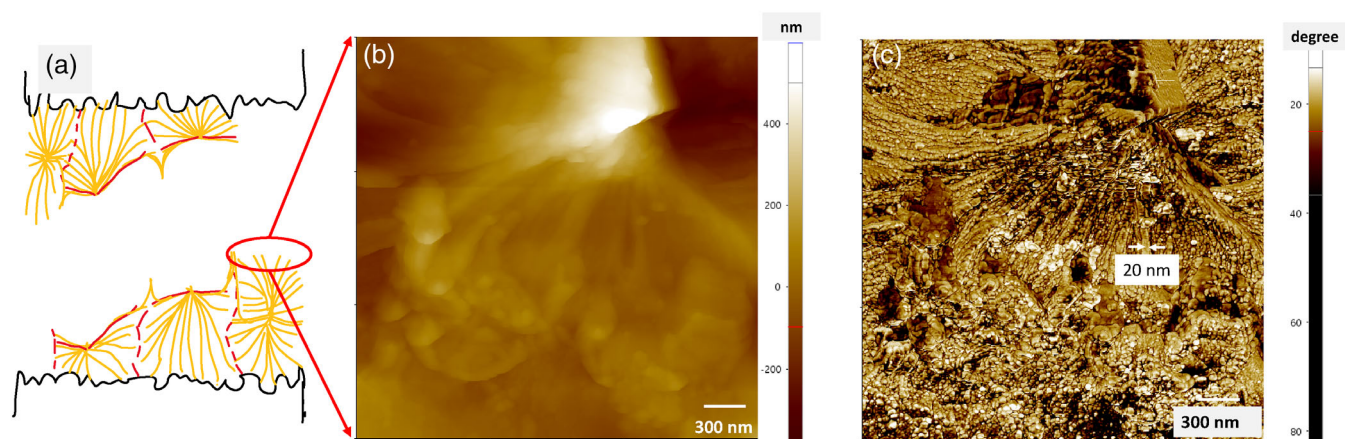
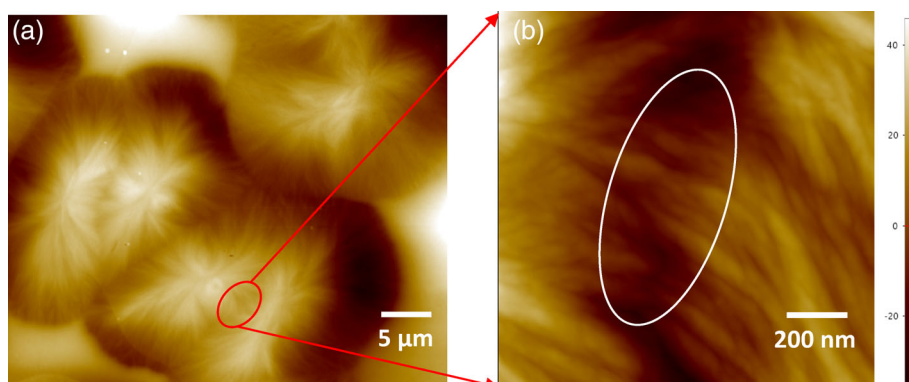


FIGURE 6 (a) Schematic drawing of the fracture of single layer polyether ketone ketone (PEKK) spherulites. (b) Atomic force microscopy (AFM) height morphology of the PEKK polymer region after adhesive failure with Ti plate surface. (c) AFM phase image corresponding to (b). [Color figure can be viewed at wileyonlinelibrary.com]

Figure 7a,b showed two different crack paths along with the two directions 1 and 2. This results indicate that when a monolayer PEKK spherulites are opened, fracture behavior of these spherulites will also be anisotropic. To confirm this, the core structure of different spherulites after opening as shown in Figure 2c were further characterized using tapping mode AFM.

As schematically shown in Figure 7g, crack paths 1 and 2 correspond to crack planes i and ii. For these two different crack planes, the crack behavior at the micro-scale is different. For crack plane i, the crystalline structure at the core of the spherulite after the crack has been characterized using the AFM phase mode as shown in Figure 3. The fracture plane is dominated by an inter-lamella fracture. For crack plane ii, as shown in Figure 7g, breaking of the lamella itself is needed, thus, involving intra-lamella cracking. The intra-lamella crack region can be recognized in Figure 7e. This anisotropic crack behavior can be observed in nature, and it can be compared to the breaking of an apple along different planes, which also has an asymmetric structure as shown in Figure 7h.

Additional fracture morphology analyses of the individual PEKK spherulites were performed using AFM. Figure 8 shows three fracture morphologies of the PEKK spherulites. Figure 8a,c,e are the phase images at the core of three different spherulites after fracturing. Figure 8b,d,f are the corresponding height images. In these experiments, the directions of the nucleation site are random, thus, the crack may occur along any direction between path 1 and path 2 as shown in Figure 7a. The intra-lamella crack region varies from 100 nm to a few μm (by a factor of 10) as shown in Figure 8a,c,e. From the corresponding height morphology, a larger amount of plastic deformation is recognized from the height difference for the intra-lamella crack regions. Since the intra-lamella strength is much larger than the inter-lamella strength, the anisotropic crack behavior of PEKK spherulites observed, suggests that the nucleation site directions need to be tailored with respect to the load direction, in order to maximize the intra-lamella failure, and further increase the overall mechanical properties of the material.

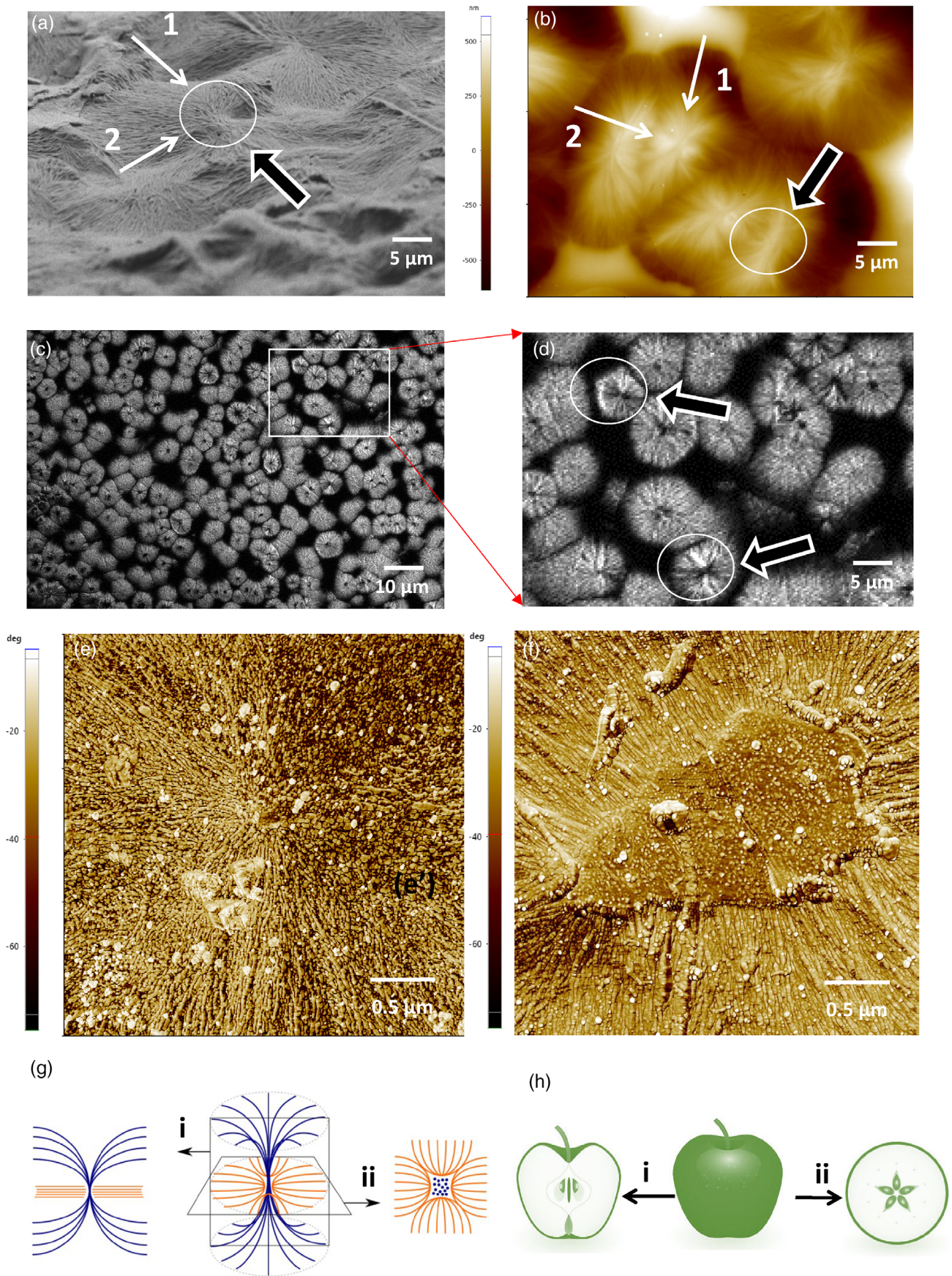


FIGURE 7 Legend on next page.

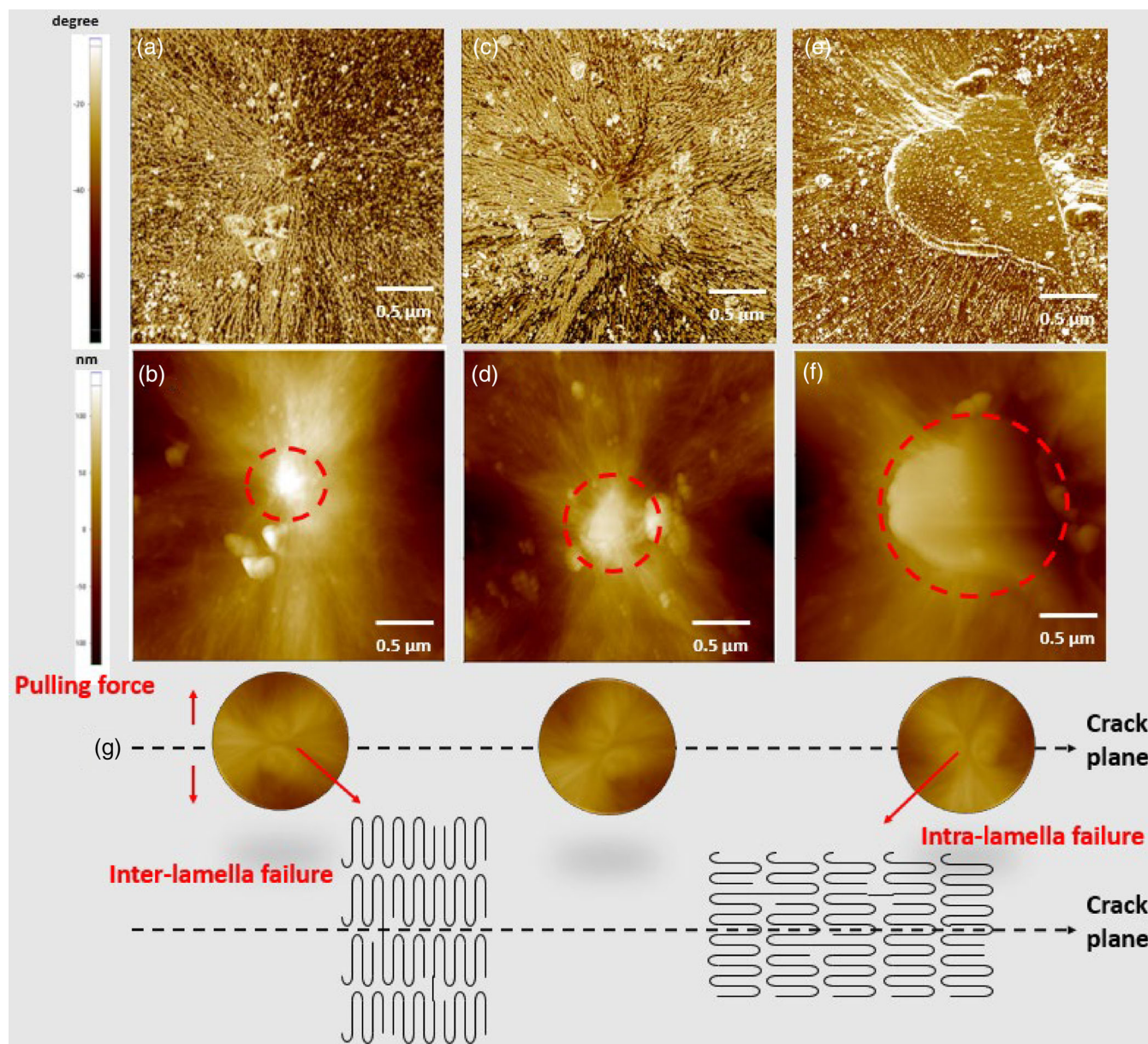


FIGURE 8 (a) Atomic force microscopy (AFM) phase image of the crack surface of a PEKK spherulite. (b) AFM height image of the crack surface of a polyether ketone ketone (PEKK) spherulite corresponding to (a). (c) AFM phase image of the crack surface of a second PEKK spherulite. (d) AFM height image of the crack surface of a PEKK spherulite corresponding to (c). (e) AFM phase image of the crack surface of a third PEKK spherulite. (f) AFM height image of the crack surface of a PEKK spherulite corresponding to (e). (g) Schematic drawing of the inter- and intra-lamella failures with respect to different crystalline packing structures at the crack plane. [Color figure can be viewed at [wileyonlinelibrary.com](https://onlinelibrary.wiley.com/doi/10.1002/app.54764)]

4 | CONCLUSION

We reported an experimental method to study the fracture of the individual PEKK spherulites. By applying a pulling

force on a thin PEKK film composed of a single layer of PEKK spherulites, the crack occurs at the core and opens the spherulites. This is a new approach to directly observing the fracture of crystalline structures at an individual

FIGURE 7 Characterization of the isotropic structure of the polyether ketone ketone (PEKK) spherulites using various methods: (a) Scanning electron microscopy image. (b) Atomic force microscopy (AFM) height morphology image. (c) Optical microscopy image. (d) High-resolution optical microscopy image of the region marked as white square in (c). (e) AFM phase image of the crack surface of a PEKK spherulite. (f) AFM phase image of the crack surface of another PEKK spherulite. (g) Schematic drawing of the anisotropic crack behavior of PEKK spherulites. (h) Schematic drawing of the anisotropic structure of an apple. [Color figure can be viewed at [wileyonlinelibrary.com](https://onlinelibrary.wiley.com/doi/10.1002/app.54764)]

spherulite level. AFM phase images of the fracture surface show an anisotropic fracture behavior, the plastic deformation region of an individual spherulite with respect to the intra-lamella failure, may vary by a factor of 10 and is determined by the direction of the nucleation site with respect to the applied force. Our results provide a deeper understanding of the fracture behavior of a spherulite and may yield a new approach to preparing crystalline structures by tailoring the nucleation site direction, for example, using 2D nucleation agents.

AUTHOR CONTRIBUTIONS

Vanessa Marinosci: Conceptualization (equal); data curation (equal); methodology (equal); writing – original draft (equal). **Kuan Chen:** Conceptualization (equal); data curation (equal); methodology (equal); writing – original draft (equal). **Nick G. J. Helthuis:** Investigation (equal); methodology (equal). **Wouter J. B. Grouve:** Conceptualization (equal); formal analysis (equal); methodology (equal); supervision (equal); writing – review and editing (equal). **Erik G. de Vries:** Formal analysis (equal); investigation (equal); methodology (equal); writing – review and editing (equal). **Ningzhong Bao:** Methodology (equal); writing – review and editing (equal). **Remko Akkerman:** Funding acquisition (equal); methodology (equal); writing – review and editing (equal). **Matthijn B. de Rooij:** Investigation (equal); methodology (equal); writing – review and editing (equal). **Liangyong Chu:** Conceptualization (equal); methodology (equal); supervision (lead); writing – original draft (lead); writing – review and editing (lead).

ACKNOWLEDGMENTS

This research was supported by the National Key Research and Development Program of China (Grant No. 2020YFE0100100) and this work is part of the research program “HTSM2017” with project number 16213, which is (partly) funded by the Dutch Research Council (NWO). The authors also gratefully acknowledge the financial and technical support from the industrial and academic partners of the ThermoPlastic composites Research Center (TPRC), as well as the support funding from the Province of Overijssel for improving the regional knowledge position within the Technology Base Twente initiative.

CONFLICT OF INTEREST STATEMENT

The authors declare no conflicts of interest.

DATA AVAILABILITY STATEMENT

The data that support the findings of this study are available from the corresponding author upon reasonable request.

ORCID

Liangyong Chu  <https://orcid.org/0000-0001-7496-4775>

REFERENCES

- [1] H. Kang, Y. Li, J. Liang, D. Thomson, H. Cui, Y. Li, *Composites Part B* **2022**, *247*, 110356.
- [2] A. Zaami, I. Baran, T. C. Bor, R. Akkerman, *Composites Part A Appl. Sci. Manufact.* **2021**, *146*, 106402.
- [3] B. I. Oladapo, S. A. Zahedi, S. O. Ismail, F. T. Omigbodun, *Colloids Surf., B* **2021**, *203*, 111726.
- [4] W. A. Pisani, M. S. Radue, S. Chinkanjanarot, B. A. Bednarczyk, E. J. Pineda, K. Waters, R. Pandey, J. A. King, G. M. Odegard, *Polymer* **2019**, *163*, 96.
- [5] D. Bassett, R. Olley, I. Al Raheil, *Polymer* **1988**, *29*, 1745.
- [6] D. Ivanov, A. M. Jonas, *Macromolecules* **1998**, *31*, 4546.
- [7] T. Choupin, B. Fayolle, G. Régnier, C. Paris, J. Cinquin, B. Brulé, *Polymer* **2018**, *155*, 109.
- [8] C. Li, A. Strachan, *Polymer* **2019**, *174*, 25.
- [9] S. Feng, C. Liu, H.-J. Sue, *Compos. Sci. Technol.* **2022**, *221*, 109298.
- [10] J.-N. Chu, J. M. Schultz, *J. Mater. Sci.* **1989**, *24*, 4538.
- [11] B. Crist, J. M. Schultz, *Prog. Polym. Sci.* **2016**, *56*, 1.
- [12] A. J. Lovinger, *Macromolecules* **2020**, *53*, 741.
- [13] H. Keith, F. Padden, *J. Polym. Sci.* **1959**, *39*, 123.
- [14] K. Saib, W. Evans, D. Isaac, *Polymer* **1993**, *34*, 3198.
- [15] Z. Chen, Y. Wang, B. Xiong, J. Zhu, *Polymer* **2020**, *203*, 122832.
- [16] H. Guo, R. G. Rinaldi, M. Broudin, S. Tayakout, O. Lame, *Polymer* **2021**, *234*, 124232.
- [17] X. Li, K. Ru, S. Zhang, Y.-K. Chen, *Polymer* **2022**, *246*, 124759.
- [18] P. Rae, E. Brown, E. Orler, *Polymer* **2007**, *48*, 598.
- [19] V. Speranza, S. Liparoti, V. Volpe, G. Titomanlio, R. Pantani, *Polymer* **2020**, *196*, 122459.
- [20] G. Kumaraswamy, A. M. Issaian, J. A. Kornfield, *Macromolecules* **1999**, *32*, 7537.
- [21] V. Marinosci, N. Helthuis, L. Chu, W. Grouve, M. de Rooij, S. Wijskamp, R. Akkerman, *Eng. Fract. Mech.* **2022**, *268*, 108475.
- [22] P. A. Klonos, M. Lazaridou, C. Samiotaki, A. Kyritsis, D. N. Bikiaris, *Polymer* **2022**, *259*, 125329.
- [23] G. Zhang, P. C. Lee, S. Jenkins, J. Dooley, E. Baer, *Polymer* **2014**, *55*, 4521.
- [24] P. Bernardo, D. Zampino, G. Clarizia, *Sep. Purif. Technol.* **2020**, *250*, 117201.
- [25] B. Dörling, A. Sánchez-Díaz, O. Arteaga, A. Veciana, M. I. Alonso, M. Campoy-Quiles, *Adv. Optical Mater.* **2017**, *5*, 1700276.
- [26] C. Dingler, K. Dirnberger, S. Ludwigs, *Macromol. Rapid Commun.* **2019**, *40*, 1800601.
- [27] X. An, W. Liu, L.-B. Bai, L.-L. Sun, M. Xu, L.-H. Xie, L. Song, C.-X. Xu, Y.-G. Yang, B. Liu, *Chem. Mater.* **2021**, *33*, 5326.
- [28] L. Ma, Z. Yan, X. Zhou, Y. Pi, Y. Du, J. Huang, K. Wang, K. Wu, C. Zhuang, X. Han, *Nat. Commun.* **2021**, *12*, 1.
- [29] V. J. Yallapragada, D. Oron, *Opt. Lett.* **2019**, *44*, 5860.
- [30] F. Detrez, S. Cantournet, R. Seguela, *Polymer* **2011**, *52*, 1998.

- [31] C. Thomas, R. Seguela, F. Detrez, V. Miri, C. Vanmansart, *Polymer* **2009**, *50*, 3714.
- [32] M.-S. Lee, E. M. Woo, *Polymer* **2019**, *166*, 88.
- [33] V. M. Marinosci, W. J. Grouve, M. B. de Rooij, S. Wijskamp, R. Akkerman, *Int. J. Adhes. Adhes.* **2021**, *109*, 102893.
- [34] L. Chu, M. Bus, A. V. Korobko, N. A. Besseling, *Ultramicroscopy* **2019**, *205*, 1.
- [35] L. Chu, A. V. Korobko, A. Cao, S. Sachdeva, Z. Liu, L. C. de Smet, E. J. Sudhölter, S. J. Picken, N. A. Besseling, *Adv. Mater. Interfaces* **2017**, *4*, 1600495.
- [36] J. E. Sader, J. W. Chon, P. Mulvaney, *Rev. Sci. Instrum.* **1999**, *70*, 3967.
- [37] L. Chu, W. J. Grouve, M. van Drongelen, E. G. de Vries, R. Akkerman, M. B. de Rooij, *Adv. Mater. Interfaces* **2021**, *8*, 2001894.
- [38] L. Chu, W. J. Grouve, M. van Drongelen, Y. Guha, E. G. de Vries, R. Akkerman, M. B. de Rooij, *Adv. Eng. Mater.* **2021**, *23*, 2000518.
- [39] S. Agbolaghi, S. Abbaspoor, F. Abbasi, *Prog. Polym. Sci.* **2018**, *81*, 22.
- [40] Q. Guan, B. Norder, L. Chu, N. A. Besseling, S. J. Picken, T. J. Dingemans, *Macromolecules* **2016**, *49*, 8549.
- [41] S. Magonov, V. Elings, M.-H. Whangbo, *Surf. Sci.* **1997**, *375*, L385.
- [42] Y. Ono, J. Kumaki, *Macromolecules* **2018**, *51*, 7629.

How to cite this article: V. Marinosci, K. Chen, N. G. J. Helthuis, W. J. B. Grouve, E. G. de Vries, N. Bao, R. Akkerman, M. B. de Rooij, L. Chu, *J. Appl. Polym. Sci.* **2024**, *141*(1), e54764. <https://doi.org/10.1002/app.54764>